SCRIT electron scattering facility

T. Ohnishi[*1] and K. Tsukada[*1,*2] for the SCRIT Collaboration

Introduction

Electron scattering has long been used as a powerful tool to precisely study atomic nuclei. This is due to several properties of electron scattering. Firstly, the interaction is well known; secondly, electron has no structure; and finally, the scattered nuclei are not disturbed. For these reasons, electron scattering has been utilized in various manner. For example, by performing elastic electron scattering experiments, the charge density distribution of a nucleus has been precisely measured. In addition, inelastic scattering, (e, ep') reaction, and other reactions have also been performed to precisely investigate the nature of excited states of a nucleus.[1)]

Electron scattering has been performed in stable nuclei of most of elements. However, there are only a few measurements of electron scattering on unstable nuclei, for example, ^{3}H, ^{14}C, and ^{41}Ca, which are long-life isotopes. The main reason is the difficulty in preparing a large amount of targets for more production-hard, short-lived unstable nuclei due to the required large luminosity for electron scattering.

Despite the present situation of electron scattering, the requirement for electron scattering off unstable nuclei, especially electron elastic scattering is increasing consistently. This is because fundamental physical quantities such as the radius and density distribution have not been well-studied in recent research on unstable nuclei. Although the nuclear charge radius is well-investigated by isotope shifts,[2)] there are no measurements of charge density distributions of short-lived unstable nuclei. Moreover, the nuclear matter radius and distribution have been studied via the reaction cross section[3)] and proton elastic scattering.[4)] Therefore, there is model dependence in the reduction process of nuclear neutron radius and neutron density distribution. This has affected the understanding of applications such as nucleosynthesis or equation of state in the field of astrophysics,[5,6)] which is one of the major themes of unstable nuclei research.

To realize electron scattering off unstable nuclei, a novel target forming method, Self-Confining Radioactive-isotope Ion Target (SCRIT), was proposed.[7)] In electron storage rings, ion trapping is a well-known phenomenon where electron beams attract ions of residual gases. When ions of unstable nuclei are used instead of residual-gas ions, they are trapped by the electron beam. The SCRIT method utilizes this idea as a static target of unstable nuclei. In addition, the SCRIT device comprises three electrodes that produce the longitudinal trapping potential along the beam direction. Consequently, ions are trapped around electron beams in three dimensions and electron scattering is automatically conducted without any precise position tuning of the electron beam.

In 2004, the development of the SCRIT method was started at KSR, Kyoto University. Following several years of development, the SCRIT method was proven in 2009.[8,9)] This allowed the construction of the SCRIT electron scattering facility at the RIKEN RI Beam Factory[10)] in 2009. RI production was started in 2013.[11)] After successful commissioning of the experiment with stable ^{132}Xe target in 2016, development of the SCRIT trap and electron scattering with unstable nuclei have been performed. As a result, the first experiment of electron scattering with online-produced unstable nuclei was conducted in 2023.[13)] This article introduces the SCRIT electron scattering facility and presents several results of the experiment.

The SCRIT electron scattering facility

The SCRIT electron scattering facility in Fig. 1 comprises an electron accelerator, Racetrack Microtron (RTM),[10)] electron storage ring, SCRIT-equipped RIKEN Storage Ring (SR2),[10)] new ISOL system, Electron-beam-driven RI separator for SCRIT (ERIS),[11)] dc-to-pulse converter, Fringing-RF-field-Activated dc-to-pulse Converter (FRAC).[14)] The SCRIT system is installed in the straight section of SR2. An electron magnetic spectrometer, Window-frame spectrometer for electron scattering (WiSES), is installed beside the SCRIT system, and a luminosity monitor system (LMon) is also installed at the downstream exit of the straight section of SR2.

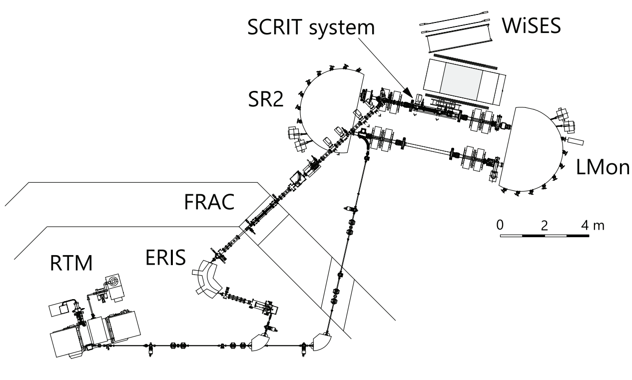

Fig. 1. Schematic of the SCRIT electron scattering facility.

*1 RIKEN Nishina Center
*2 Institute of Chemical Research, Kyoto University

DOI:10.34448/RIKEN.APR.57-902

RTM and SR2

RTM and SR2 have been used since long called AURORA-III at Sumitomo Heavy Industries, Ltd. to study the accelerator techniques. In 2009, they were moved to the SCRIT facility, as illustrated in Fig. 2.

Fig. 2. Photographs of a) RTM and b) SR2 at the SCRIT electron scattering facility.

RTM is a compact microtron used as an electron beam injector for both SR2 and ERIS, which accelerates the electron beam to 150 MeV. During injection to SR2, the electron beam power is approximately 0.4 W at a 2-Hz repetition rate. For RI production, the pulse width of the electron beam is extended from 2 to 4 μs, average current is approximately 2 mA, and repetition rate is increased to 20 Hz, which increases the electron beam power to approximately 20 W.

SR2 is an electron storage ring, where the electron beam energy can be varied from 100 to 700 MeV depending on the experimental requirement. The typical storage beam current and lifetime are 300 mA and 1 Ah, respectively. The electron beam size at the SCRIT device is approximately 2 and 0.4 mm (σ) in the horizontal and vertical directions, respectively.

ERIS

ERIS is the first ISOL facility to be fully developed at RIBF, as illustrated in Fig. 3, and comprises a production target, transfer tube, an ion source, and a beam-analyzing transport line. ERIS provides RI beam using the photofission reaction of uranium driven by the electron beam. This reaction is effective for the production of more neutron-rich isotopes around the tin isotopes compared with other fission reactions.[15)]

The production target are self-made thin uranium carbide disks. There are several merits to this approach: 1) Using a thin target disk, the release efficiency from the target is expected to be improved due to the large surface area and short distance for diffusion. 2) Vapor pressure and density of uranium carbide are lower and higher than those of uranium oxide, respectively. 3) Damages to the material in the ion source are reduced due to the small amount of oxygen. Uranium oxide and graphite powders were manually ground and formed into a disk without using a binder, but only pressing under a high pressure of approximately 180 MPa. Subsequently, the formed disk was converted into a uranium carbide disk at approximately 1100–1600°C by the carbothermal reduction. The obtained disk was 18 mm in diameter and 0.8 mm in thickness. The average mass concentration of the uranium in the disk was estimated to be 3.4 g/cm^3. The production-target disks were installed inside a graphite container, and tantalum disks with a thickness of 5 mm and diameter of 20 mm were also inserted in front of the production target to increase the production of γ rays, as illustrated in Fig. 4. The graphite container was surrounded with a tantalum heater, and it was connected to the ion source through a transfer tube. For fast effusion and diffusion, all components were heated to approximately 2000°C. Further details of uranium carbide disk are described in Ref. 16).

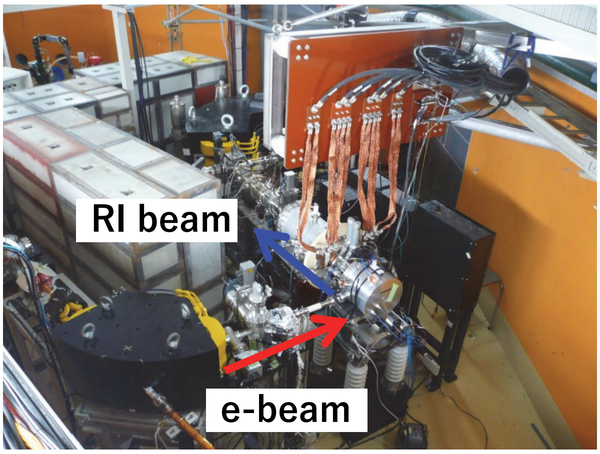

Fig. 3. Photograph of ERIS.

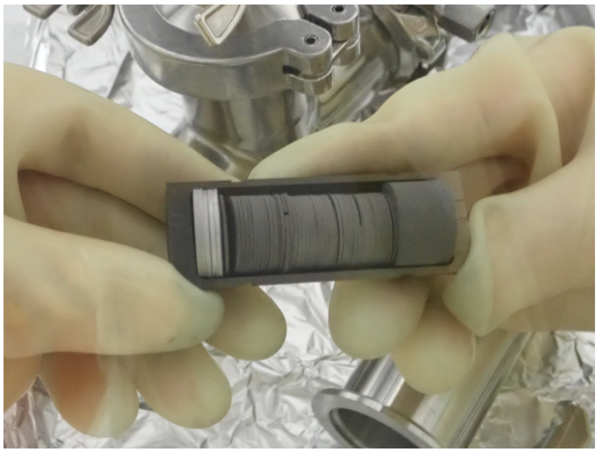

Fig. 4. Photograph of uranium carbide target.

At ERIS, two types of ion sources are used, because the ionization method depends on the target chemical element. One is a forced-electron beam induced arc discharge (FEBIAD) type ion source and the other is a surface ionization type ion source. The FEBIAD type ion source is used for a wide range elements with large ionization potential. The surface ionization type ion source is used for mainly alkaline and alkaline earth elements. The grid electrodes are equipped with both ion sources for stacking inside the ion source. The ion source is placed on a high-voltage stage (<50 kV) for acceleration, and ion beams are produced. Details of ions sources are described in Ref. 17).

In the beam transport line, mass separation is performed, and the maximum magnetic rigidity of the bending magnet is 0.96 Tm. As a result of the commissioning, the mass resolution was obtained as approximately 1600 in σ.[11)]

FRAC

Using the ion beam from ERIS, dc-to-pulse conversion is required for injection into the SCRIT system. In addition, a low-emittance ion beam is required for long-line beam transport to the SCRIT system. For these requirements, FRAC was installed between ERIS and the SCRIT system.

FRAC is based on RF quadrupoles and comprises six quadrupoles electrodes, a set of einzel lenses, injection, extraction, and barrier electrodes. Details of FRAC are described in Ref. 14). For high conversion efficiency and cooling of accumulated ions, the pressure inside FRAC is maintained at approximately 10^{-3} Pa with a relatively small amount of neon buffer gas during operation. To extract a short pulse of approximately 300 μs width, the potential inside FRAC is decreased towards the exit electrode to approximately -45 V, and ions are accumulated near the exit electrode. The capacity of the ions with this operation condition is approximately 10^8 ions with a large RF-amplitude of 1 kV_{pp}.

SCRIT system

Figure 5 illustrates a schematic of the SCRIT system, which comprises the SCRIT device, scrapers for measuring the ion beam located in front of the SCRIT device, and the analyzing system for the trapped ions located under the SCRIT chamber. Further details can be found in Ref. 10).

The SCRIT device comprises a main electrode and two barrier electrodes. The main electrode comprises two 3-mm thick electrodes at the top and bottom and thin 0.1-mm thick meshed electrodes on both side walls. The line width of the mesh is approximately 0.1 mm, and the mesh pitch is 8 and 5 mm in the horizontal and vertical directions, respectively. No mesh is stretced horizontally over the 35-mm center of the vertical direction to allow scattered electrons to penetrate. The inner size of the main electrode is approximately 99 (h) $\times$ 115 (w) $\times$ 780 (d) mm^3. The barrier electrodes are birdcage-shaped racetrack electrodes made

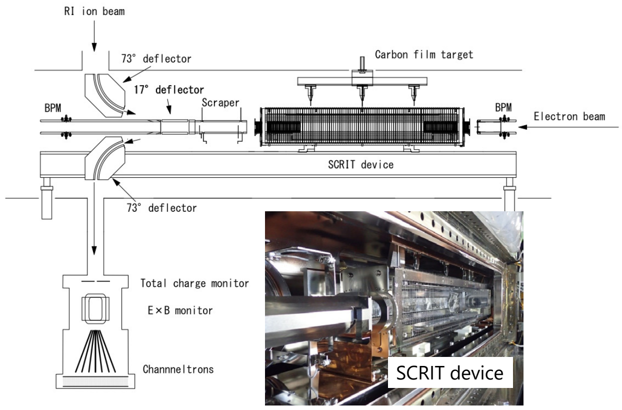

Fig. 5. Schematic of the SCRIT system. A picture of the SCRIT system, particularly the SCRIT device, in the vacuum chamber is included in the figure.

of wire, with a 0.2-mm diameter. They are incorporated into both ends of the main electrode through insulators, and are used to generate the barrier potentials.

Ion injection and extraction are controlled by switching the entrance barrier potential. After trapping inside the SCRIT device for an amount of time that can be varied (the trapping time), the trapped ions are extracted and transported to a total charge monitor and analyzer system comprising an E $\times$ B velocity filter and 43 channeltrons. The total charge monitor works as slits at the analyzer system to achieve suitable resolution of the mass-to-charge ratio. The total charge and charge state distribution of the target ions inside the SCRIT device are measured for each trap. Recent developments of the analyzer system are reported in Ref. 18).

Detector system

Electrons scattered from target ions confined in the SCRIT device are emitted through a 2 mm-thick beryllium window and are detected by WiSES which was installed at its current position in 2014 as illustrated in Fig. 6. WiSES comprises a dipole magnet with a large gap of 1700 (w) $\times$ 290 (h) $\times$ 1400 (l) mm^3; two drift chambers, called the front drift chamber (FDC) and rear drift chamber (RDC); 2-m long plastic scintillation counters for trigger generation; and a helium bag covering the entire volume between the two drift chambers. The FDC and RDC each have eight planes with XX'YY'XX'YY' configuration and ten planes with UU'VV'XX'UU'VV' configuration, respectively. The X plane provides horizontal information of the scattered electron trajectory, and the U, V and Y planes are tilted by 45°, -45°, and 90°, respectively, with respect to the X plane. In both drift chambers, each cell has a hexagonal shape with a side length of 10 mm. The drift chambers are filled with

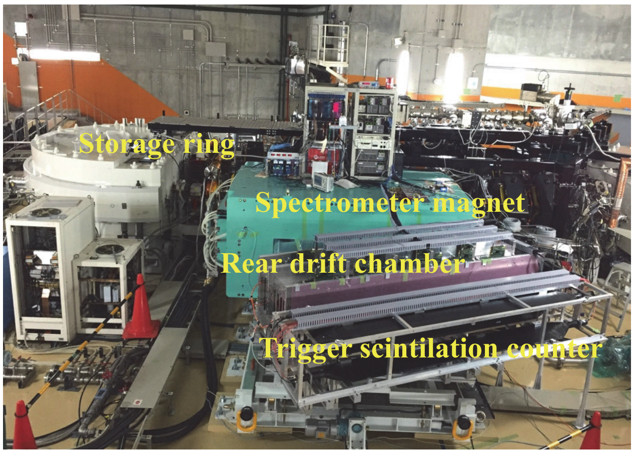

Fig. 6. Photograph of storage ring (SR2) and electron magnetic spectrometer (WiSES).

He : C_2H_6 (80 : 20) gas.

The trajectories of the scattered electrons are reconstructed by the two drift chambers to derive the momenta, scattering angles, and reaction vertex points. The magnetic field is 0.8 T for an electron beam energy of 300 MeV. The solid angle of the spectrometer is approximately 80 mSr, covering a scattering angle from 30° to 60°. The momentum resolution is $\delta p/p \sim 1 \times 10^{-3}$ for an electron beam energy of 300 MeV.

The luminosity is continuously monitored by counting bremsstrahlung photons with LMon comprising a pure CsI calorimeter array to measure the photon energy, and a plastic scintillation fiber array to measure the spatial distribution as illustrated in Fig. 7. The cross section of each pure CsI crystal is a regular hexagon with 40 mm on each side, and the length is 20 cm corresponding to 11 radiation lengths. Six out of seven segments surround the central one. The bremsstrahlung photons are collimated to a diameter of 50 mm by a 50 mm-thick lead collimater, and mainly irradiated onto the central CsI crystal.

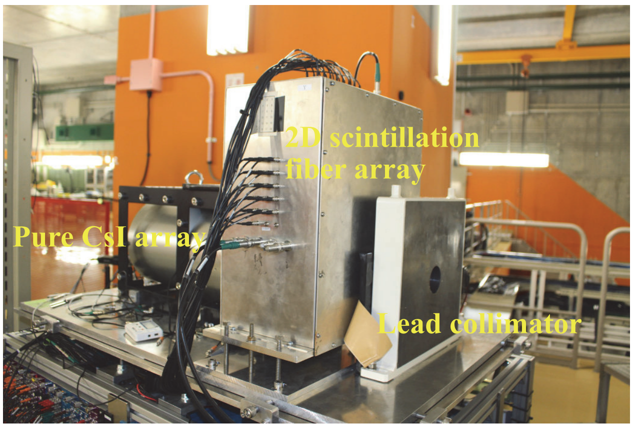

Fig. 7. Photograph of luminosity monitor (LMon).

We have conducted electron scattering experiments for several targets, and some results from three experiments are presented in this report.

Commissioning experiment with carbon target

Carbon has been commonly used as a target for electron scattering in various facilities because of its ease of preparation and handling, resulting in a good understanding of its nuclear properties such as the charge density distribution.[24] In the SCRIT system, there are three 25 μm-thick carbon foils positioned at the center and ±250 mm from the center along the electron beamline, as illustrated in Fig. 5, to assess the spectrometer's performances. These carbon targets are normally moved outside the SCRIT device by remote operation. During electron scattering experiments, the carbon targets are initially shifted to the halo region and then gradually moved to the center of the electron beam to maintain a constant reaction rate corresponding to the decrease in the beam current. Figure 8 illustrates the reconstructed momentum spectrum within a scattering angle range of 50° to 55° for an electron beam energy of 300 MeV. As depicted in the figure, one elastic and two inelastic peaks are distinctly separated.

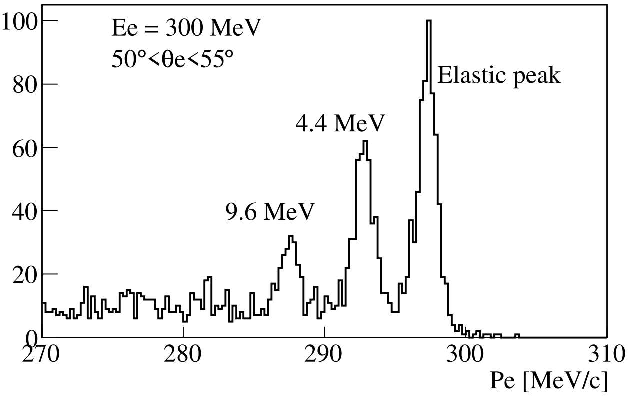

Fig. 8. Momentum spectrum within the scattering angle between 50° and 55° for the carbon target. The electron beam energy is 300 MeV.

Performance

RI beam production

In this section, two results of the RI beam production using different ion sources are reported. In both RI production experiments, RI beams are transported to the particle identification (PID) system located at the exit of FRAC. The PID system comprises a rotating disk and Ge detector. PID was performed by measuring specific γ-rays corresponding to the decay of the stopped RIs using a Ge detector. The measured rates were estimated from the number of observed γ-rays based on the efficiency of the Ge detector and half-life of each isotope.

First results were observed using the FEBIAD type ion source. In total, 23 uranium carbide target disks were used and the total amount of uranium was about 15 g. The irradiation beam power was approximately 10 W, and the target temperature was maintained at approximately 2000°C. The generated RI beams were accelerated to 20 keV. The observed rates for ^{132}Sn and ^{138}Xe were 2.6×10^5 and 3.9×10^6 atoms/sec, respectively. Comparing the obtained rate with the expected production rate inside the target yields the overall efficiency including the release efficiency from the target, ionization efficiency inside the ion source, and transport efficiency of the beam line. The overall efficiencies for ^{132}Sn and ^{138}Xe were found to be 2.1% and 5.5%, respectively. Details of this measurement is described in Ref. 19).

Another result concerns RI beams produced using the surface ionization type ion source. In total, 48 uranium carbide target disks were used and the total amount of uranium was approximately 28 g. The electron beam power was approximately 15 W. In the surface ionization method, the ionization chamber was heated to approximately 1600°C using the registive heating method. Cesium isotopes are mainly ionized in this temperature range. The ionized RI were accelerated to 6 keV. The production rate of ^{137}Cs was estimated to be 1×10^5 atoms/s with an electron beam power of 1 W. Detail can be found in Ref. 20).

Pulse beam production

Dc-to-pulse conversion was performed using a two-stage stacking of ERIS and FRAC for injection into the SCRIT system. The first-stage stacking was performed within ERIS and stacked RI beams were extracted with a 500-μs time window. The stacking and extraction voltages of the exit grid were 100 and -180 V, respectively. The frequency dependence of the first-stage stacking inside ERIS was studied using a ^{140}Cs beam. The stacking efficiency is defined as the ratio of the number of stacked ions to that of a continuous beam. The stacking efficiency was close to 0.8 at 40 Hz operation of ERIS. Further details of the first-stage stacking are described in Ref. 21). The second-stage stacking was performed with FRAC. The injection into FRAC was synchronized with the extraction from ERIS. At the injection of a new pulsed ion beam from ERIS, almost zero escape of stacked ions from FRAC was achieved by adjusting the entrance barrier potential of FRAC, because the energy of the last injected ion became sufficiently lower than the energy of the newly injected ion due to the collision with neon buffer gas during a 25-ms cooling time at 40-Hz operation of ERIS. The accumulated ions were extracted from FRAC with a 300-μs pulse width after several seconds of accumulation, and almost zero leakage of the accumulated ions from FRAC was confirmed.

Performance of the SCRIT method

One of the indications of the performance of the SCRIT method is the trap efficiency ϵ_{trap} and overlap efficiency ϵ_{over}. The trap efficiency is estimated by $\epsilon_{trap} = N_{trap}/N_{inj}$, where N_{inj} is the number of injected ions measured at the scraper in front of the SCRIT device, and N_{trap} is the number of trapped ions. N_{trap} is estimated from the measured total charge and average charge state at the analyzer system. The effective number of ions, N_{coll}, colliding with the electron beams, can be estimated from the measured luminosity. The overlap efficiency is given by $\epsilon_{over} = N_{coll}/N_{trap}$.

Figure 9 illustrates the electron-beam current dependence of the trap efficiency ϵ_{trap} and overlap efficiency ϵ_{over} for Ba ions with a 200-ms trapping time at 150 MeV. In the measurement, a stable ^{138}Ba ion beam accelerated to 6 keV was produced from ERIS, and a pulsed ion beam was injected into the SCRIT device using the FRAC stacking. The beam intensity was typically 2.3×10^8 ions/pulse. After the trapping in the SCRIT device, extracted Ba ions were transported to the total charge monitor and the analyzer system. From the measured charge state distribution, Ba^{4+} ion is dominant, and the average charge state is estimated to be 3.6. The trap efficiency increased almost linearly with beam current from 130 to 230 mA, and it saturated, reaching approximately 42%. This saturation indicates the escape of the highly charged state ions. The overlap efficiency is approximately 42% at 200 mA, in contrast to the previous result which yielded an overlap efficiency of 15% at 200 mA with a

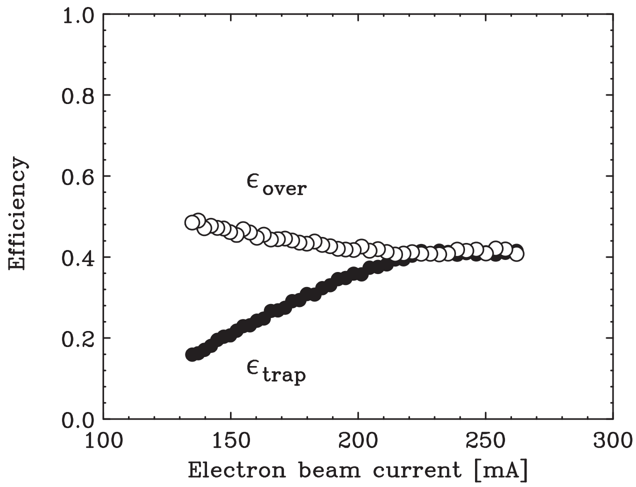

Fig. 9. Electron beam current dependence of the trap efficiency and overlap efficiencies with 200-ms trapping time at 150 MeV.

50-ms trapping time. This increase indicates that the spatial distribution of the highly-charged-state ions is smaller than that of the low charge state ions, and closer to the electron beam size.

These results demonstrates the dynamics of the trapped ions inside the SCRIT device, which are significantly different from the ion-trap technique using electron beams, EBIT.[22] For more detailed studies, a new analyzer system is being developed that allows us measuring the spatial distribution of ions in each charge state, which helps to understand the motion of trapped ions.

The dependence of the luminosity on the electron beam current was measured at 150 and 250 MeV using an ^{136}Xe ion beam; 2.5 × 10^8 ions/pulse of ^{136}Xe were injected into the SCRIT device at a trapping time of 250 ms. Figure 10 shows the result of the current dependence. A luminosity of approximately 3.2 × 10^{27} cm^{-2}s^{-1} was achieved at 250-mA beam current and 250-MeV beam energy.

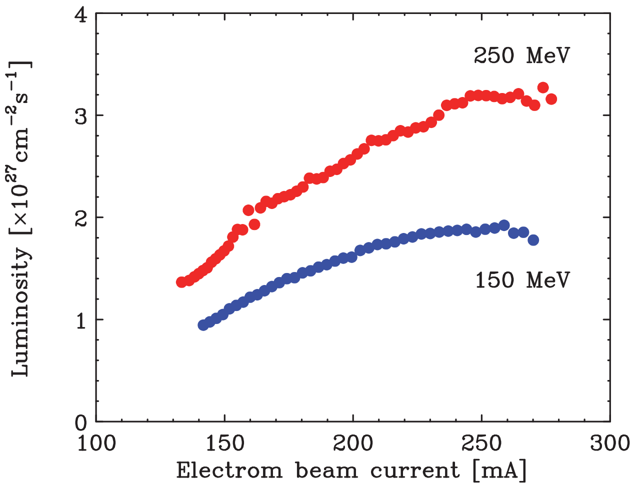

Fig. 10. Electron beam current dependence of the luminosity. Red and blue circles show the results of for electron-beam energies of 150 and 250 MeV, respectively.

Experiments at the SCRIT facility

Xe isotope targets

A series of experiments with xenon isotopes have been intermittently conducted recent years, covering isotopes from ^{124}Xe to ^{136}Xe, including the neutron magic nucleus ^{136}Xe, and will extend to ^{138}Xe after a facility upgrade. These data will demonstrate the capability of the SCRIT facility to explore isotope dependencies across the neutron magic numbers from the perspective of charge density distribution. For stable isotopes, natural xenon gas is introduced into ERIS and ionized using the FEBIAD method. At the SCRIT system, the trapping time is 200 ms or 250 ms, with alternating conditions with and without target ions. Figure 11 presents preliminary results, including those for ^{132}Xe target, which have already been published.[12] Electron beam energies were selected to sufficiently cover the diffraction pattern for extracting the charge density distribution of the nucleus, assuming a two parameter Fermi distribution. Data for $^{124\text{–}134}$Xe in the higher momentum transfer region will be obtained in the near future.

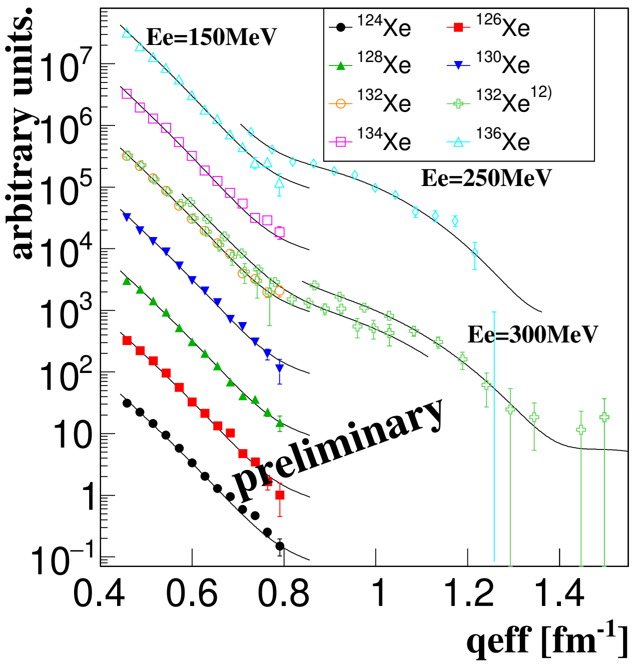

Fig. 11. Momentum transfer dependence of the obtained cross sections for Xe isotopes so far. Vertical positions are scaled for clarity.

^{137}Cs target

As previously described, unstable cesium isotopes were successfully extracted as the ion beam using a newly developed surface ionization ion source at ERIS and the beam stacking method by FRAC. The ^{137}Cs beam was accumulated in the FRAC for 4 sec, yielding approximately 10^7 ions/pulse extraction. The main contamination in the cesium beam was barium isotope at ERIS, and the purity of ^{137}Cs beam was evaluated to be more than 99.5%. At the SCRIT system, the trapping time was 1.9 sec with a 0.1 sec interval. The electron beam energy was 149 MeV and average electron beam current was 200 mA. The achieved luminosity for ^{137}Cs was 0.9 × 10^{26} cm^{-2}s^{-1}. Figure 12 shows the obtained angular distributions for ^{137}Cs and the background, primarily originating from residual gases in SR2. The momentum transfer region from 0.4 to 0.7 fm^{-1} is covered. The lines represent theoretical calculations using a phase shift code DREPHA,[25] assuming a two-parameter Fermi distribution with a

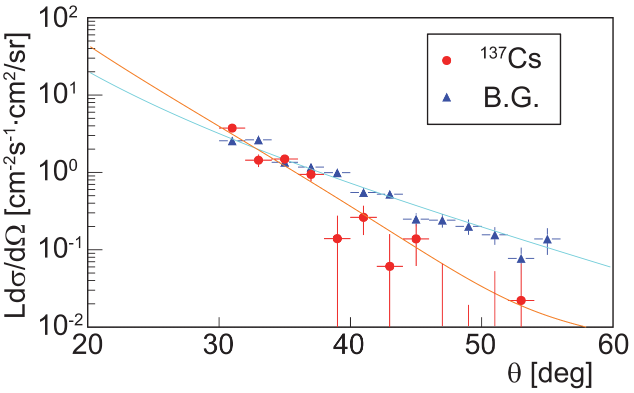

Fig. 12. Angular distribution for ^{137}Cs and background. Lines are theoretical calculations by a phase shift code DREPHA.

charge radius of $\sqrt{\langle r\rangle^2} = 4.813$ fm[23] and diffuseness of $t = 2.3$ fm for ^{137}Cs, while a three parameter Gauss distribution of ^{16}O[24] is assumed for the background. The measured angular dependence are reproduced well by the calculations, because the cross section is dominated by the electric monopole component of the elastic scattering process in the low-momentum transfer region, despite ^{137}Cs having a spin parity of $I^P = 7/2^+$ in its ground state.

Future plan

The success of the world's first electron scattering with online-produced unstable nuclei marks a milestone for the SCRIT project. The upgrade of the SCRIT facility is underway for the next stage, which is electron scattering with the short-lived nucleus, ^{132}Sn. ^{132}Sn is an iconic nucleus in the study of unstable nuclei due to its double magic number, $Z = 50$ and $N = 82$. Main upgrades are the increase in the electron beam intensity for RI production, and improvement of the SCRIT trap for high efficiency.

The objective value for the increased electron beam power is approximately 2 kW, aiming to produce 10^8 atoms/sec of ^{132}Sn. Moreover, several improvements are underway to realize the required power: The repetition rate and peak current of RTM will be increased by upgrading the modulator power supply. In addition, an upgrade of the radiation shield and development of the remote handling system of ERIS are also planed. Concerning the improvement of the SCRIT method, there are plans to update the monitoring system of the SCRIT trap and develop a new RF cavity of the electron storage ring to stabilize the SCRIT trap.

As future project, the measurement of 4th-order moment is proposed using electron elastic scattering of unstable nuclei. This measurement should aid in deducing the information of the mean square radius of the point-neutron distribution based on recent theoretical works.[26] The 4th-order moment can be deduced precisely using the measurement data at the low-momentum transfer region where the cross section is large. This character is very useful for the case of unstable nuclei.

In the present, the SCRIT electron scattering facility has started to establish and develop the study of unstable nuclei by electron scattering. In other facilities, electron scattering of unstable nuclei is only mentioned for future plans. Therefore, the SCRIT electron scattering facility will lead this research field.

References

1) T. Suda and H. Simon, Prog. Part. Nucl. Phys. **96**, 1 (2017) and references therein.
2) I. Angeli, At. Data Nucl. Data Tables **87**, 185 (2004).
3) A. Ozawa, "Matter Radii and Density Distributions," in *Handbook of Nuclear Physics*, (Springer, Singapore, 2022).
4) H. Sakaguchi and J. Zenihiro, Prog. Part. Nucl. Phys. **97**, 1 (2017).
5) T. Kajino *et al.*, Prog. Part. Nucl. Phys. **107**, 109 (2019).
6) C. A. Bertulani and J. Valencia, Phys. Rev. C **100**, 015802 (2019).
7) M. Wakasugi, T. Suda, and Y. Yano, Nucl. Instrum. Methods Phys. Res. A **532**, 216 (2004).
8) M. Wakasugi *et al.*, Phys. Rev. Lett. **100**, 164801 (2008).
9) T. Suda *et al.*, Phys. Rev. Lett. **102**, 102501 (2009).
10) M. Wakasugi *et al.*, Nucl. Phys. Instr. Meth. B **317**, 668 (2013).
11) T. Ohnishi *et al.*, Nucl. Instrum. Methods Phys. Res. B **317**, 357 (2013).
12) K. Tsukada *et al.*, Phys. Rev. Lett. **118**, 262501 (2017).
13) K. Tsukada *et al.*, Phys. Rev. Lett. **131**, 092502 (2023).
14) M. Wakasugi *et al.*, Rev. Sci. Instrum. **89**, 095107 (2018).
15) Y. Ts. Organessian *et al.*, Nucl. Phys. A **701**, 87c (2002).
16) T. Ohnishi *et al.*, Proc. HIAT2015, Yokohama, Japan, (2015), p. 194.
17) T. Ohnishi *et al.*, Nucl. Instrum. Methods Phys. Res. B **463**, 290 (2020).
18) R. Ogawara *et al.*, Nucl. Instrum. Methods Phys. Res. B **541**, 90 (2023).
19) T. Ohnishi *et al.*, PoS(INPC2016)088, (2016).
20) Y. Abe *at al.*, RIKEN Accel. Prog. Rep. **55**, S19 (2022).
21) T. Ohnishi *et al.*, RIKEN Accel. Prog. Rep. **53**, 110 (2020).
22) A. N. Antonov *et al.*, Nucl. Instrum. Methods Phys. Res. A **637**, 60 (2011).
23) I. Angeli and K. P. Marinova, At. Data Nucl. Data Tables **99**, 69 (2013).
24) H. de Vries, C. W. de Jager, and C. de Vries, At. Data Nucl. Data Tables **36**, 495 (1987).
25) B. Dreher, *A phase-shift calculation code for elastic electron scattering*, communicated by J. Friedrich.
26) H. Kurasawa and T. Suzuki, Prog. Theor. Exp. Phys. **2019**, 113D01 (2019).